Traveling waves, two-phase fingers, and eutectic colonies in thin-sample directional solidification of a ternary eutectic alloy

Silvère Akamatsu and Gabriel Faivre
Groupe de Physique des Solides, CNRS UMR No. 7588, Universités Denis Diderot et Pierre et Marie Curie, Tour 23, 2 place Jussieu, 75251 Paris Cedex 05, France
(Received 9 September 1999)

We present an experimental investigation of the morphological transition of lamellar eutectic growth fronts called ''formation of eutectic colonies'' by the method of thin-sample directional solidification of a transparent model alloy, CBr_4-C_2Cl_6. This morphological transition is due to the presence in the melt of traces of chemical components other than those of the base binary alloy (impurities). In this study, we use naphthalene as an impurity. The formation of eutectic colonies has generally been viewed as an impurity-driven Mullins-Sekerka instability of the envelope of the lamellar front. This traditional view neglects the strong interaction existing between the Mullins-Sekerka process and the dynamics of the lamellar pattern. This investigation brings to light several original features of the formation of eutectic colonies, in particular, the emission of long-wavelength traveling waves, and the appearance of dendritelike structures called two-phase fingers, which are connected with this interaction. We study the part played by these phenomena in the transition to eutectic colonies as a function of the impurity concentration. Recent theoretical results on the linear stability of ternary lamellar eutectic fronts [Plapp and Karma, Phys. Rev. E **60**, 6865 (1999)] shed light on some aspects of the observed phenomena.

PACS number(s): 81.30.Fb, 05.70.Ln

I. INTRODUCTION

The solidification microstructure of directionally solidified nonfaceted binary eutectic alloys usually consists of a regular stacking of lamellae of the two eutectic crystal phases [1,2]. This microstructure is the trace left behind in the solid by the stationary periodic pattern assumed by the growth front during solidification [3]. The order of magnitude of the pattern wavelength, or interlamellar spacing λ, is fixed by the competition between solute diffusion in the liquid and capillarity, and is of 10 μm for growth velocities in the $\mu m\,s^{-1}$ range. An example observed in thin-sample directional solidification of the transparent eutectic alloy CBr_4-C_2Cl_6 is shown in Fig. 1. Necessary conditions for such a growth pattern to be observed are that the alloy concentration C be sufficiently close to the center of the eutectic plateau, and the solidification rate V smaller than a limit value, which is a function of C and the applied thermal gradient G [1–3]. These conditions define the zone of the parameter space in which the growth front is lamellar and planar (planar-growth zone), the word ''planar'' applying not to the front itself, but to its envelope, i.e., its shape smoothed over a distance of a few λ. The growth pattern of Fig. 1 is not only planar, but also stationary, symmetrical, and bidimensional, or nearly so. This type of pattern is called ''basic'' in contradistinction to other types of planar patterns with a lower symmetry (tilted and oscillatory patterns) [4–10].

In this paper, we report the results of an experimental study of the morphological instability called ''formation of eutectic colonies,'' which corresponds to the upper bound of the planar-growth zone when C is close to the eutectic concentration C_E of the alloy. This instability consists of the appearance of large cells—''eutectic colonies'' (EC's)—superimposed on the lamellar pattern (Fig. 2), and is due to the presence of impurities with a small solubility in the solid phases [11]. Metallurgical studies performed around 1960 led to the following conclusion, at least implicitly [12–15]: the formation of EC's is an impurity-driven Mullins-Sekerka instability occurring on a scale much larger than λ, and therefore essentially insensitive to the dynamics of the lamellar pattern. This conclusion seemed to be supported by the fact that, like the usual Mullins-Sekerka bifurcation [16,17], the transition from planar fronts to EC's generally occurs at values of V close to the theoretical constitutional supercooling velocity V_{cs} of the system [18]. It was noted in these old studies that the lamellar pattern adapts itself to the presence of EC's in such a way that the trajectories of the lamellae remain locally perpendicular to the distorted front (Cahn's rule [19]), without the consequences of this fact being drawn.

The similarity between EC's and dilute-alloy cells is unquestionable, but leaves aside the most interesting aspects of the formation of EC's, namely, those involving the interaction between this process and the dynamics of the underlying lamellar pattern. Cahn's rule means that the distortions of the

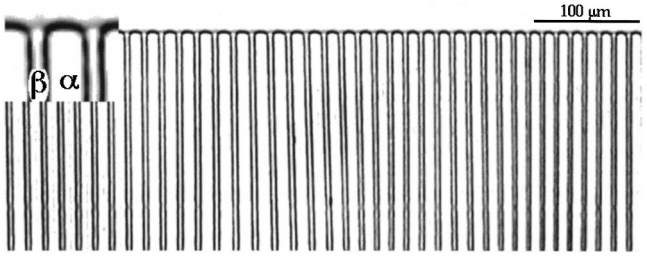

FIG. 1. Planar lamellar eutectic front in a basic (i.e., stationary symmetrical) state. Undoped CBr_4-C_2Cl_6 alloy ($\upsilon = 0.02$; $V = 1.5\,\mu m\,s^{-1}$). α and β are the two terminal solid solutions of the alloy. In this photograph, as in all the following ones, the growth direction is upward. Inset: enlarged view of the front.

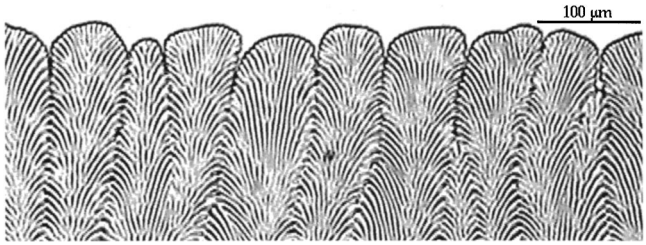

FIG. 2. Eutectic colonies in a CBr_4-C_2Cl_6-naphthalene alloy ($C_{naph}=5\times10^{-4}$; $V=31\,\mu m\,s^{-1}$). At this small value of λ (≈4 μm), the β lamellae cannot be resolved, and appear as single dark lines in the image.

front associated with a modulation of the impurity concentration field entail modifications of the λ distribution. The existence of a feedback of the λ distribution on the front shape follows from the fact that the average temperature of the front depends on λ (Jackson-Hunt's law) [3]. Because of this interaction, the formation of EC's must exhibit a much richer dynamics than the formation of dilute-alloy cells (for a detailed experimental study of the latter, see Ref. [20]). This conclusion was recently asserted by Plapp and Karma in conclusion of a linear stability analysis of the basic lamellar patterns of ternary eutectics based on Cahn's hypothesis [21]. It is experimentally substantiated by this study for the first time, to our best knowledge.

The process of formation of EC's is sensitive to relatively small changes in the impurity concentration, the deviation of the base binary alloy from C_E, and the initial value of λ, as will be seen below. A detailed quantitative study of this process would require a more accurate control of these parameters than is currently achievable. In this paper, we only claim to present a clear, semiquantitative characterization of some robust new aspects of the process. Even to this limited aim, the standard experimental methods had to be improved considerably. In thin-sample directional solidification, we recall, a layer of a transparent model alloy enclosed between two glass plates is placed in an externally imposed unidirectional temperature gradient, and pulled at an imposed velocity toward the cold side of the gradient. The front—which remains immobile, or nearly so, in the laboratory reference frame—is continuously observed with an optical microscope. This method has often been applied to the fundamental study of lamellar eutectic growth [3,9,10,22–26]. The principal nonstandard aspects of our experimental methods are that we employ very thin (≈10 μm thick) samples, and grow large (>1 mm) ''floating'' eutectic grains (see Sec. II C). This endows the system with three important characteristics—a complete crystallographic homogeneity, a low capillary anisotropy, and a pronounced two-dimensional (2D) character—without which the dynamics of lamellar eutectics are of a disconcerting complexity. With very thin, large-grained samples, it was possible to determine the full 2D stability diagram of CBr_4-C_2Cl_6 inside the planar-growth zone experimentally [10]. The experimental results were in quantitative agreement with the numerical results obtained for the same system (i.e., bidimensional CBr_4-C_2Cl_6 without capillary anisotropy) by Karma and Sarkissian [6], confirming that our samples really have the above characteristics. Another feature of the samples used in this study is that their residual-gas content was much lower than in most previous studies. A ternary chemical component had to be added in order that impurity-induced phenomena appear within the explored range in V/G. The ternary component used in this study is naphthalene. EC's were only found to form in CBr_4-C_2Cl_6-naphthalene alloys with a molar fraction of naphthalene C_{naph} larger than about 5×10^{-4}. Other impurity-induced phenomena, but no standard EC's, are observed at lower concentrations of naphthalene. This relatively sharp transition as a function of the impurity concentration is one of the unexpected findings of this study.

The plan of the paper is as follows. Previous results concerning the dynamics of lamellar eutectics, in particular, the results of the linear stability analysis of ternary eutectics by Plapp and Karma, are recalled in Sec. II. Section III is devoted to experimental methods. In Sec. IV we present preliminary observations about phase diffusion in the absence of an impurity, serving as a reference for the observations made in the presence of impurity. The results concerning the impurity-driven effects are reported in Sec. V. This section includes a comparison of the experimental observations with Plapp and Karma's theoretical results. A general conclusion is given in Sec. VI.

II. BACKGROUND

A. Binary eutectic alloys

Two essential dynamical features of binary lamellar eutectics are the absence of a mechanism of selection of the spacing, and the ineffectiveness of phase diffusion at low pulling velocities. These properties explain the important experimental fact that basic patterns never have a uniform λ distribution, but contain smooth, relatively ample spatial modulations of λ inherited from the early stages of the growth [9,25]. Let us briefly sum up the present state of our knowledge on these subjects.

The basic patterns of binary lamellar eutectics are stable over a finite range in λ at fixed values of the control parameters [6–10]. The bounds of this range essentially depend on two variables, namely, the reduced deviation from eutectic concentration $\upsilon=(C-C_E)/(C_\beta-C_\alpha)$, where C_α and C_β are the concentrations of the α and β solid phases bounding the eutectic plateau, respectively, and the reduced spacing $\Lambda=\lambda/\lambda_{JH}$ where λ_{JH} (the Jackson-Hunt minimum-undercooling spacing) is a scaling length proportional to $V^{-1/2}$. At $\upsilon=0$, the basic patterns are stable for Λ ranging from about 1 to 2. Below $\Lambda\approx1$, they are unstable against lamella termination. Above $\Lambda\approx2$, they undergo a homogenous bifurcation to a period-preserving oscillatory ($1\lambda O$) pattern, followed by a secondary bifurcation to a period-doubling oscillatory ($2\lambda O$) pattern at a slightly higher value of Λ. At slightly off-eutectic concentrations ($|\upsilon|\approx0.04$), the bifurcation sequence is reversed (the primary bifurcation is the $2\lambda O$ one). At still higher values of Λ and/or υ, a tilt bifurcation also comes into play.

The average temperature of a binary lamellar eutectic front, or, equivalently, the position ζ of the envelope along the axis of the thermal gradient (z axis), depend on the value of λ. When λ is uniform, the relationship between ζ and λ is approximately given by the Jackson-Hunt equation, which reads

$$\zeta = -\frac{\Delta T_{\mathrm{JH}}}{2G}(\Lambda + \Lambda^{-1}), \tag{1}$$

where the origin is taken at the eutectic temperature, and ΔT_{JH} (the Jackson-Hunt minimum undercooling) is a scaling quantity proportional to $V^{1/2}$ [3]. In the experiments, the spatial distribution of λ is generally not uniform, is associated with a nonplanar envelope of the front, and is nonstationary. The linear stability analysis of a modulated lamellar eutectic front of average spacing λ_0 was performed by Datye and Langer [4] under the assumption that Cahn's rule is obeyed. This rule states that the motion of each trijunction point is submitted to the constraint $\xi_t^{(n)} + V\zeta_x = 0$, where t is the time, x is the coordinate parallel to the front, and $\xi^{(n)}$ is the x coordinate of the nth trijunction point. From this, it is easily derived that

$$\lambda_t + \lambda_0 V \zeta_{xx} = 0, \tag{2}$$

where λ is considered as a continuous function of x. Equations (1) and (2) are the equations governing the spatiotemporal evolution of the two functions $\lambda(x,t)$ and $\zeta(x,t)$. Following the usual linear-stability analysis procedure, one finds that the linear growth coefficient $\Omega(k)$ of a small perturbation of wave vector k obeys a second-order equation. Only one of the solutions of this equation is relevant in the conditions of the experiments to be described in Sec. IV, and corresponds to a diffusive mode, i.e., a mode such that $\lambda(x,t)$ follows a diffusion equation $\lambda_t = D_{\mathrm{ph}}\lambda_{xx}$, where D_{ph} is the so-called phase diffusion coefficient. D_{ph} reads

$$D_{\mathrm{ph}} = \frac{\Delta T_{\mathrm{JH0}} V}{2G}(\Lambda_0 - \Lambda_0^{-1}) \tag{3}$$

(the Cahn-Datye-Langer equation), where the subscript 0 refers to the nonperturbed stationary state of uniform spacing λ_0. The most striking aspect of this equation is that the sign of D_{ph} changes at $\Lambda_0 = 1$, which means that the lamellar pattern grows unstable below this value of Λ. As mentioned, lamella termination events, which are probably the ultimate outcome of such an instability, have indeed been experimentally observed to occur at, or at least a little below, $\Lambda = 1$. In Sec. IV, our interest will not be in this instability, but in the phase diffusion process that occurs at values of Λ noticeably larger than 1. It will be kept in mind that the Cahn-Datye-Langer is a linearized equation, which is valid only when the amplitude of the λ gradients are vanishingly small. When this condition is not fulfilled, Eq. (3) can only be utilised to estimate the order of magnitude of the damping rate of the λ modulations.

B. Multicomponent eutectic alloys

The results of the Plapp-Karma stability analysis of ternary eutectics can be summed up as follows [21]. The simplifying assumptions made in the calculation are the same as in Datye and Langer's previous work, i.e., they mostly amount to Cahn's hypothesis. It is found that the Cahn-Datye-Langer diffusive branch is not significantly modified by the presence of an impurity as long as V is much smaller than V_{cs}. However, on approaching V_{cs}, this branch mixes with the Mullins-Sekerka branch of the envelope. Like a standard Mullins-Sekerka branch, the mixed branch presents a broad maximum at a wavelength much longer than λ, but, contrary to what occurs in dilute alloys, this branch may be complex near the maximum—in other words the critical, or nearly critical, long-wavelength perturbations may be drifting (or oscillating). Plapp and Karma carried out a detailed study of the conditions under which $\Omega(k)$ is real, or, on the contrary, complex, in the region of the long-wavelength maximum. Unfortunately, our experiments cannot cross-check their predictions in detail. We can only state that, in the conditions of our experiments ($\Lambda > 1.5$, $V > V_{\mathrm{cs}}$), Ω is probably always complex in the ranges in k and V of interest.

Plapp and Karma calculated the critical velocity for the long-wavelength mode of ternary eutectics (i.e., the velocity V_c above which the maximum of the real part of Ω is positive), and established that V_c is given by an approximate formula quite similar to the Mullins-Sekerka formula for the critical velocity of dilute alloys. For the sake of clarity, let us reproduce this well-known formula in the case of a dilute binary alloy CBr_4-naphthalene. The partition coefficient of naphthalene is denoted K_{naph}, the liquidus slope m_{naph}, and the diffusion coefficient in the liquid D_{naph}. The same symbols with a subscript X, will be used in the case of the system CBr_4-X, where X is the residual gas. The thermal gap of the alloy is $\Delta T_{\mathrm{naph}} = m_{\mathrm{naph}}(K_{\mathrm{naph}}^{-1} - 1)C_{\mathrm{naph}}$, the thermal length $1_{\mathrm{th}} = \Delta T_{\mathrm{naph}}/G$, and the capillary length $d_0 = a_0/\Delta T_{\mathrm{naph}}$ where a_0 is the Gibbs-Thomson capillary coefficient. To a good approximation, V_c is given by the constitutional-supercooling velocity $V_{\mathrm{cs}} = D_{\mathrm{naph}}1_{\mathrm{th}}$ multiplied by a ''capillary-correction factor'' denoted $1 + V_{\mathrm{cl}}/V_{\mathrm{cs}}$. The capillary-correction term is $V_{\mathrm{cl}}/V_{\mathrm{cs}} = 1.5(2K_{\mathrm{naph}}d_0/1_{\mathrm{th}})^{1/3}$. In most experiments, $d_0/1_{\mathrm{th}} \ll 1$, and the capillary-correction term is relatively small. However, it must be kept in mind that $d_0/1_{\mathrm{th}}$ increases rapidly as the solute concentration decreases. The system becomes absolutely stable when $V_{\mathrm{cl}}/V_{\mathrm{cs}}$ reaches a value close to 1.

In the case of ternary eutectic alloys, Plapp and Karma showed that ΔT_{naph} must be replaced by an effective thermal gap ΔT_{eff}, which depends on the partition coefficients and the liquidus slopes of the impurity with respect to the two eutectic crystal phases. These quantities are not known in our case, so we shall assume that they are equal to the known quantities pertaining to the dilute CBr_4-X and CBr_4-naphthalene systems (see Sec. III A). The formulas for V_{cs} are then the same as in a dilute alloy. In the case of a ternary dilute alloy CBr_4-naphthalene-X, the constitutional-supercooling velocity is $V_{\mathrm{cs}} = G/(\Delta T_{\mathrm{naph}}/D_{\mathrm{naph}} + \Delta T_X/D_X)$. Taking for C_X the highest value found in our samples (4×10^{-4}), and $G = 110\ \mathrm{K\,cm^{-1}}$, we obtain $V_{\mathrm{cs}} \simeq 3/(1 + 4 \times 10^3 C_{\mathrm{naph}})\ \mu\mathrm{m\,s^{-1}}$. The thus obtained values of V_{cs} are compared with the measured instability threshold velocities of planar fronts below. It will be seen that the calculated and the measured quantities are within a factor of 2 or 3 of each other, which is satisfactory given the rough approximations made in the calculations, and the large experimental uncertainty. We also note that, according to the above formula, the influence of the highest residual-gas concentration is comparable to that of a molar fraction of 2.5×10^{-4} of naphthalene. This explains the variability of the threshold velocities observed in the low impurity concentration range.

Concerning the leading-order correction term to V_{cs}, Plapp and Karma showed that d_0 must be replaced by an effective value d_{eff} which includes a term which is not of a capillary origin, but represents the stabilizing effect of the interlamellar diffusion field. In our case, Plapp and Karma's formula gives values of V_{cl}/V_{cs} which are of a few 10^{-2} at $C_{naph} \geqslant 5\times10^{-4}$, but larger than 10^{-1} at $C_{naph} \leqslant 2.5\times10^{-4}$. This large value of V_{cl}/V_{cs} is perhaps the origin of the surprisingly high instability threshold velocities found in low impurity concentration samples.

The long-wavelength Mullins-Sekerka-like mode is not the only mode of instability of the planar lamellar eutectic fronts. As already stated, in the absence of impurity, the lamellar pattern is unstable to various oscillatory or tilt modes for certain values of V, Λ, and υ. Of these modes, only the $2\lambda O$ one is compatible with Cahn's rule, at least approximately, and was found by Datye and Langer. Plapp and Karma showed that the presence of an impurity greatly enhances the $2\lambda O$ mode, suggesting that, in some cases, the destabilization of the planar front may occur through the $2\lambda O$ mode rather than the long-wavelength mode. Observations supporting this view are reported below.

C. Anisotropy effects. Eutectic grains

Eutectic fronts are composed of crystallographic domains called eutectic grains [27]. The crystal orientation in the lamellae of the two solid phases is uniform within a eutectic grain, and varies from a eutectic grain to another. The capillary anisotropy of the system (i.e., the orientation dependence of the surface tensions of the α-liquid, β-liquid, and α-β interfaces) is different in different grains. In a previous study, a classification of the eutectic grains of our system according to their capillary anisotropy was established [25]. In the so-called locked grains, the direction of growth of the lamellae is locked onto a preferential orientation, corresponding, most probably, to a sharp minimum of the surface tension of the α-β interface. The grains in which no such locking is observed were called ''floating'' grains. It was shown that, in these grains, the growth dynamics is similar to that of a system without capillary anisotropy as calculated numerically [6], except for the small capillary-anisotropy effects to be described shortly. A method of obtaining large floating grains was applied in this study (see Sec. III B).

If no capillary anisotropy at all was present, the system would be symmetrical with respect to the z axis, and the lamellae would run parallel to this axis when the system is in a basic pattern. However, since some capillary anisotropy is actually present, the mirror symmetry of the system is broken in most eutectic grains, and, even in the basic patterns, the lamellae run at a small angle ϕ (the anisotropy-driven tilt angle) from the z axis. This angle is a function of the orientation of the grain, and, in a given grain, increases as λ increases. In the floating grains of CBr_4-C_2Cl_6, the value ϕ_m of ϕ at the reference value of the spacing λ_{JH} is generally less than 2°, but ϕ increases relatively rapidly as λ increases because of the spontaneous tilt bifurcation undergone by the system at large values of λ. Since ϕ is different in different grains, the two patterns on either side of a eutectic grain boundary have different values of ϕ. Consequently, lamellae are repeatedly terminated, or created at eutectic grain boundaries, which are therefore permanently surrounded by steep local λ gradients. These gradients may act as sources of traveling dynamical defects. In particular, eutectic grain boundary λ gradients are permanent sources of traveling waves in the presence of impurities at sufficiently high V (see Sec. V C 1).

III. EXPERIMENTAL METHODS

A. Products and samples

The samples are made of two parallel glass plates separated by plastic spacers, delimiting an empty space about 8 mm wide, 70 mm long, and 12 μm thick. The alloys are prepared by mixing zone-refined CBr_4, C_2Cl_6, and naphthalene. The mixing process is carried out under a low pressure of argon. A fragment of the solidified mixture deposited at one end of a heated empty sample remelts, and fills the sample by capillarity. The filled samples are placed in an externally imposed thermal gradient, and pulled with a dc motor via a micrometric screw. During the pulling, the growth front is continuously observed with an optical microscope over the whole width of the selected eutectic grain. The images are recorded with the help of a CCD camera and a videotape recorder, and then analyzed with a computer [28]. In the present study, the value of G is 110 $\mathrm{K\,cm^{-1}}$ unless otherwise stated. The scanned range of V is 0.9–31 $\mu\mathrm{m\,s^{-1}}$.

In this study, the concentration of the base binary alloy CBr_4-C_2Cl_6 is C_E to within experimental uncertainty ($\approx\pm0.003$), unless otherwise mentioned. The above scaling quantities are $\lambda_{JH}V^{1/2} = 14\ \mu\mathrm{m^{3/2}\,s^{-1/2}}$ and $\Delta T_{JH}V^{-1/2} = 0.033\ \mathrm{K}\,\mu\mathrm{m^{-1/2}\,s^{1/2}}$ to within about 20% [26]. Alloys without naphthalene (undoped alloys), and alloys doped with molar fractions of naphthalene of 2.5×10^{-4}, 5×10^{-4}, and 10^{-3} are used. The samples also contain residual gases, which we admit to consist of a single component X, introduced during the mixing and filling processes. The partition coefficient ($K_X \approx 0.02$), the liquidus slope ($m_X \approx 50$ K per molar fraction), and the liquid-phase diffusion coefficient ($D_X \approx 300\ \mu\mathrm{m^2\,s^{-1}}$) of X in CBr_4 have been determined [29]. C_X was found to vary from a sample to another depending on the care with which the outgasing, mixing, and filling processes were carried out, but was at most of 4×10^{-4}. In the present study, C_X was generally markedly lower than this values, as shown by the weakness of the impurity-induced effects at high V in most undoped samples. A rough experimental determination of the partition coefficient ($K_{naph} \approx 0.07$), the liquidus slope ($m_{naph} \approx 300$ K per molar fraction), and the liquid-phase diffusion coefficient ($D_{naph} \approx 300\ \mu\mathrm{m^2\,s^{-1}}$) of naphthalene in CBr_4 has been performed by the same methods as in Ref. [29].

B. Grain boundary effects

Considering the great complexity of the dynamics of lamellar eutectics, it is obviously desirable that the samples be as homogeneous as possible. The two main sources of nonhomogeneity are the presence of several eutectic grains, and the nonuniform λ distribution of the initial state (see Sec. IV). In a previous study, a method of obtaining samples containing a single floating eutectic grain was successfully ap-

plied to hypereutectic samples [10]. In brief, this method consists of preceding the experimental runs by a short preliminary pulling at a very low value of V during which the lateral invasion of the front through which the lamellar pattern is created is controlled. The same method was applied in this study, but turned out to be less efficient near the eutectic concentration than far from it. We could not grow single-grain samples, but were nevertheless able to obtain grains of millimetric sizes.

C. V jump method

Basically, the experimental procedure that we follow is that of upward V jumps. First, the growth front is put in a stationary planar basic state by pulling a long time at a low velocity V_1, and then the pulling velocity is suddenly switched to a higher velocity V_2 at which some morphological instability is expected to occur. V jumps of moderate amplitude do not change the average spacing $\langle\lambda\rangle$, generally, and thus change the average reduced spacing $\langle\Lambda\rangle$ by a factor of $\sqrt{V_2/V_1}$. Since the instability threshold of the planar front can only be reached through upward V jumps, $\langle\Lambda\rangle$ is always relatively high (>1.5) in this study.

V jumps are followed by long solute redistribution transients [30]. During the initial solute redistribution transient, the naphthalene concentration ahead of the front increases from C_{naph} to the steady-state value $C_{\mathrm{naph}}/K_{\mathrm{naph}}$. The characteristic time of the transient is $\tau_{\mathrm{naph}}=D_{\mathrm{naph}}/(K_{\mathrm{naph}}V^2)$, and the corresponding solidified length $l_{\mathrm{naph}}=D_{\mathrm{naph}}/(K_{\mathrm{naph}}V)$. After a V jump from V_1 to V_2, the concentration ahead of the front rises above the steady-state value, and then returns to this value with a characteristic time $D_{\mathrm{naph}}/(K_{\mathrm{naph}}V_1V_2)$. The amplitude of the post-jump concentration overshoot depends on V_2/V_1, but may be quite large even for moderate values of V_2/V_1 when the partition coefficient of the solute is small, which is our case.

If no V jump is applied, i.e., if the pulling is entirely performed at constant V (the short preliminary stage at a lower V can be neglected as far as solute redistribution is concerned), the destabilization of the planar front can only be observed in the course of initial transients at values of V higher than the instability threshold. The order of magnitude of the time after which the destabilization is observed is τ_{naph}. It will be seen below that the order of magnitude of the instability thresholds is of 1 $\mu\mathrm{m\,s^{-1}}$ in our system. The corresponding transients are very long (typically $\tau_{\mathrm{naph}}\approx 3$ h and $l_{\mathrm{naph}}\approx 1$ cm). Therefore, only very few different values of V could be explored with a given sample, limiting the accuracy with which instability thresholds could be measured. The values given below are the lowest value of V at which a destabilization was observed, and are probably substantially higher than the corresponding theoretical transition velocities.

On the other hand, large upward V jumps can be used to provoke a transitory increase of the impurity concentration at the front, and hence a transient destabilization of the planar front. This technique was used in order to establish the metastable character of planar fronts at low impurity concentration.

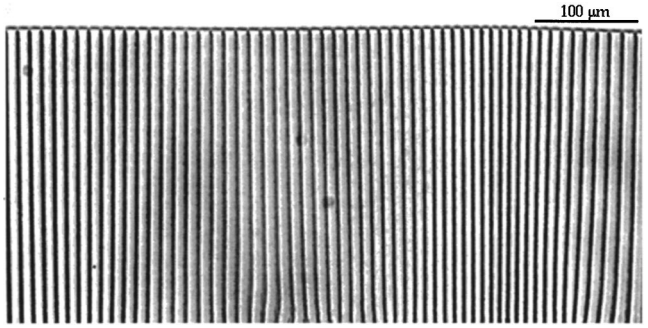

FIG. 3. Lamellar pattern with a strongly nonuniform λ distribution ($C_{\mathrm{naph}}=0$; $V=4.1\ \mu\mathrm{m\,s^{-1}}$; $G=0.005\ \mathrm{K}\,\mu\mathrm{m^{-1}}$).

IV. PRELIMINARY OBSERVATIONS

Before considering the effect of impurities on the dynamical properties of lamellar eutectic fronts, we go back over the dynamics in the absence of impurities. The initial basic patterns (i.e., the patterns obtained at the end of the preliminary stage of the pulling) contain a spatial modulation of λ with a characteristic wavelength of a few tenths of λ, and an amplitude practically equal to the width of the basic-state stability range. In previous studies performed at $V\approx 1\ \mu\mathrm{m\,s^{-1}}$ and $G\approx 10^{-2}\ \mathrm{K}\,\mu\mathrm{m^{-1}}$, the distortions of the front associated with this nonuniform grown-in λ distribution were not detected, and phase diffusion was found to be ineffective [9,25]. At the relatively high values of V which we are now able to reach without impurity-driven effects thanks to the higher purity of our samples, these effects can be measured. A detailed study is currently in progress. In view of what follows, it is useful to present the following preliminary observation here.

Figure 3 shows an undoped sample pulled at $V=4.1\ \mu\mathrm{m\,s^{-1}}$ under a thermal gradient of about $5\times 10^{-3}\ \mathrm{K}\,\mu\mathrm{m^{-1}}$. The snapshot was taken a few seconds after the onset of the pulling, when residual-gas effects (if any) are small. The distortion of the front, although hardly visible in Fig. 3, was easily measurable on the computer screen. Figure 4 shows $\lambda(x)$ and $\zeta(x)$ measured along the front, and the function $\zeta_{\mathrm{calc}}(x)$ calculated by inserting the measured values of $\lambda(x)$ into the Jackson-Hunt equation. It

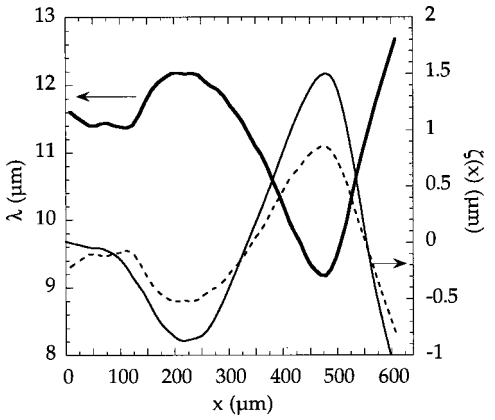

FIG. 4. Measured spacing distribution $\lambda(x)$ (thick line) and front shape $\zeta(x)$ (thin line) for Fig. 3. Dotted line: calculated value of $\zeta(x)$. For the latter quantity, the origin is taken at the average position of the front.

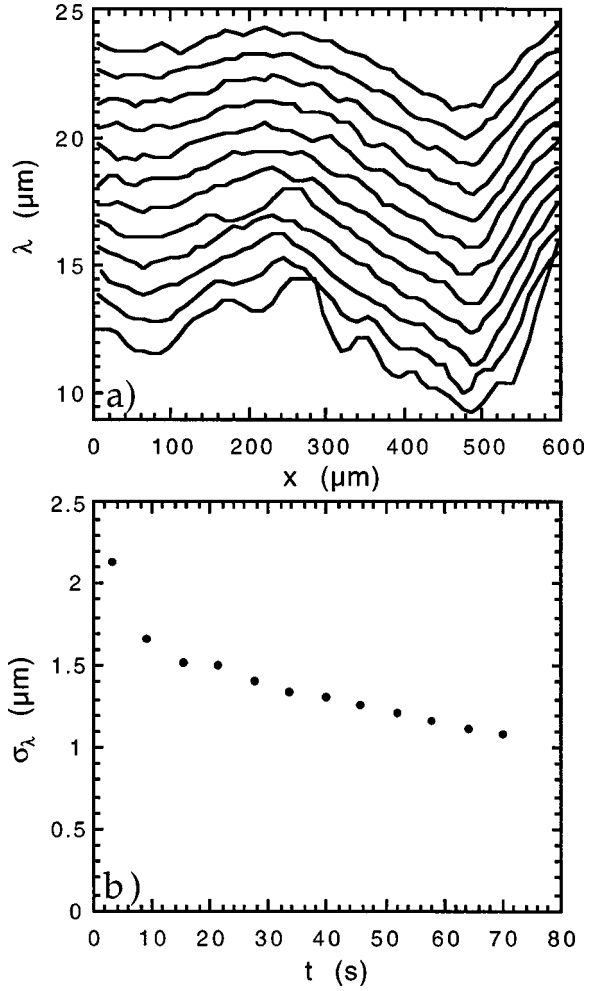

FIG. 5. (a) $\lambda(x)$ measured from Fig. 3 at time intervals of 6.1 s. The last λ plot is the same as in Fig. 4. For clarity, the successive plots have been shifted along the ordinate axis by an arbitrary quantity (1 μm). (b) Standard deviation σ_λ of $\lambda(x)$ as a function of time.

can be seen that the ratio $\zeta(x)/\zeta_{\mathrm{calc}}(x)$ is constant and of the order of unity. Figure 5(a) shows a time series of λ plots extracted from Fig. 3. The λ distribution is progressively damped out without any lateral drift. Figure 5(b) shows the time evolution of the standard deviation σ_λ of the λ distribution. An exponential law fitted to the terminal part of $\sigma_\lambda(t)$ gives a damping coefficient of about $7\times10^{-3}\,\mathrm{s}^{-1}$. Noting that, near the end of the process, the Fourier transform of the λ distribution is peaked around 25 $\langle\lambda\rangle$, we have calculated the phase-diffusion damping coefficient $D_{\mathrm{ph}}k^2$ for the mode of wavelength $2\pi/k=25\langle\lambda\rangle$ [see Eq. (3)]. The value found is of about $2\times10^{-2}\,\mathrm{s}^{-1}$, in relatively good agreement with the measured value. These results strongly suggest that the terminal stage of the damping process is essentially due to the Cahn-Datye-Langer phase-diffusion mechanism. Similar observations were made in samples containing naphthalene, showing that even relatively large impurity concentrations do not qualitatively modify the dynamics of lamellar eutectic fronts at sufficiently low V. A more extensive comparison with the predictions of the Cahn-Datye-Langer equation based on a larger set of experimental data is currently in progress.

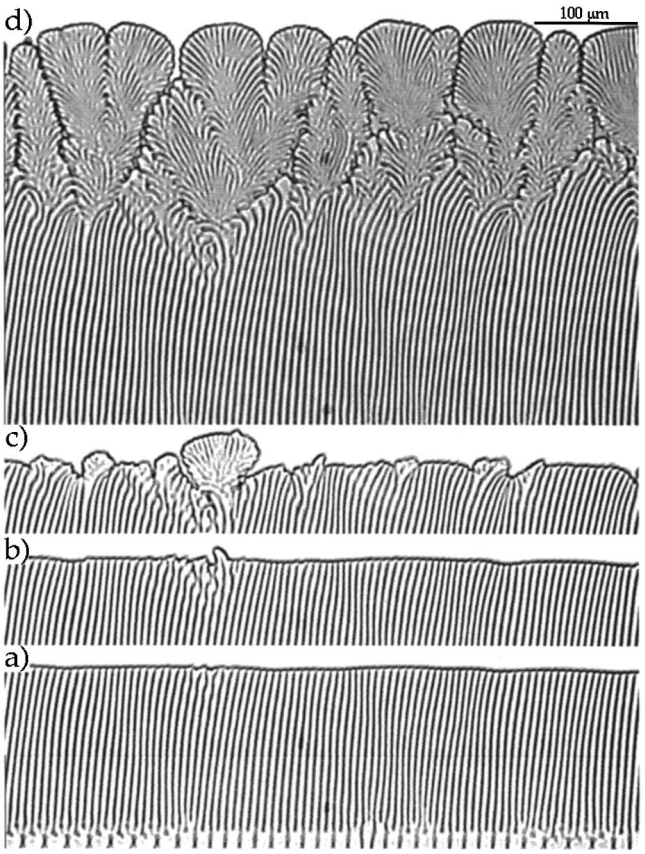

FIG. 6. Snapshots taken during the transient leading to the eutectic colonies of Fig. 2 at times (a) $t=11.9$ s, (b) 13.0 s; (c) 14.8 s, and (d) 18.9 s. A velocity jump from 0.9 to 31 $\mu\mathrm{m\,s}^{-1}$ was applied at time $t=0$ [bottom of (a)].

V. IMPURITY-DRIVEN DYNAMICAL PHENOMENA

A. Overview

We begin with a brief enumeration of our findings, which will be used to introduce some nonstandard terms. As already stated, the phenomena observed in the samples with $C_{\mathrm{naph}}=0$ or 2.5×10^{-4} are different from those observed in the samples with $C_{\mathrm{naph}}=5\times10^{-4}$ or 10^{-3}. For the sake of simplicity, we call these two concentration ranges the ''low'' and ''high'' impurity concentration ranges, respectively.

High impurity concentration

(1) At high impurity concentration, EC's always appear above a velocity V_{EC} which is comparable to the calculated value of V_{cs}, in conformity with the observations reported in the metallurgical literature.

(2) Two unexpected phenomena occur during the transients prior to the formation of EC's. The first of them is the appearance of traveling waves (TW's), i.e., small-amplitude long-wavelength deformations drifting laterally at a finite velocity (Fig. 6). Surprisingly, these TW's do not grow in amplitude in the course of time, and play no essential part in the transition to EC's.

(3) The second new phenomenon is the appearance of protruding local structures baptized ''two-phase fingers'' [Figs. 6(b) and 6(c)]. This turns out to be an essential intermediate stage of the transition to EC's. It occurs after the excitation of a short-wavelength mode of instability of the

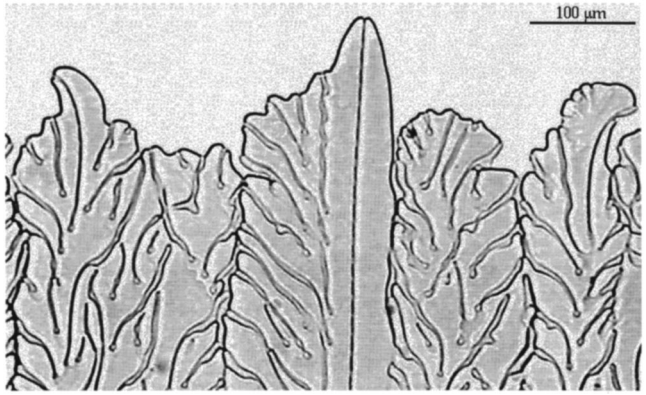

FIG. 7. α-β-α two-phase fingers and eutectic colonies in an undoped hypoeutectic ($\upsilon \simeq -0.14$) sample. $V = 4.1\ \mu\mathrm{m\,s^{-1}}$.

lamellar pattern, the nature of which depends on the initial λ distribution. This mode is sometimes, but not always, the $2\lambda O$ mode.

(4) Large-amplitude, quasistable two-phase fingers are observed to coexist with EC's at slightly off-eutectic concentrations (Fig. 7), suggesting that periodic arrays of two-phase fingers may be stationary states of the system.

(5) Once formed, the EC's are subjected to tip-splitting and squeezing-off mechanisms, leading to a rough selection of the average EC size. No steady state is reached on the scale of the individual EC's after long solidification times, suggesting that EC patterns are intrinsically unsteady.

Low impurity concentration

(6) At low impurity concentration, no spontaneous transition to EC's is observed within the explored range in V/G (Fig. 8). The value of V_{EC} (if such a velocity still exists) is thus much larger than V_{cs}.

(7) Above a velocity close to V_{cs}, planar fronts are metastable against the formation of small-amplitude (''shallow'') EC's (Fig. 9). The dynamics of the shallow-EC patterns is characterized by a very large dispersion of the EC size, and rectilinear trajectories of the inter-EC grooves, strongly suggesting that the latter are localized entities separated from each other by large portions of metastable planar or wavy front.

(8) TW's are emitted near the eutectic grain boundaries above a velocity V_{TW}, which is also close to V_{cs} (Fig. 10). The TW's are progressively damped out as they propagate

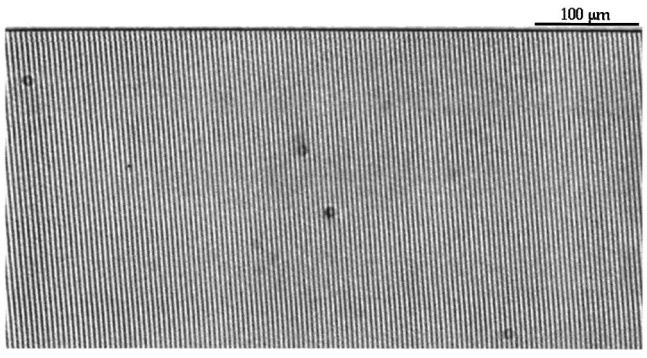

FIG. 8. Planar lamellar eutectic front at high velocity ($C_{naph} = 2.5\times10^{-4}$; $V = 31\ \mu\mathrm{m\,s^{-1}}$; $\Lambda \simeq 1.9$).

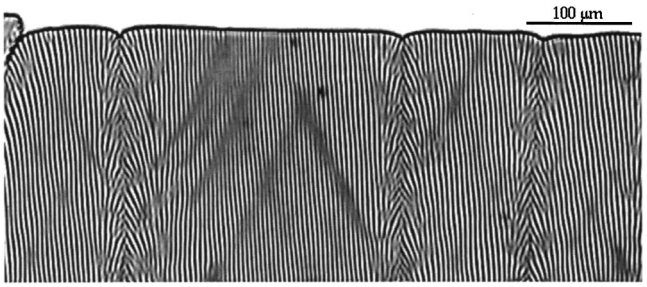

FIG. 9. Shallow eutectic colonies ($C_{naph} = 2.5\times10^{-4}$; $V = 31\ \mu\mathrm{m\,s^{-1}}$).

along the front, but their damping time is long compared to the known characteristic times of the system, especially, the phase diffusion time (see Sec. V C 3). At high V, two different situations are observed at a sufficiently large distance from the eutectic grain boundaries, depending on the efficiency of the latter as sources of TW's, namely, a perfectly planar front (Fig. 8), or a dense population of rightward and leftward TW's (Fig. 11). By ''wavy front'' we define any dynamical state in which an essentially planar front is continually swept by finite-amplitude TW's.

B. High impurity concentration

1. Transition to eutectic colonies

A series of long-duration runs at constant V were performed in samples with $C_{naph} = 5\times10^{-4}$ and 10^{-3}. In some of these runs, the front remained planar up to the end of the run, while in others EC's appeared in the course of the initial transient. We obtained $2.5 < V_{EC} < 3.2\ \mu\mathrm{m\,s^{-1}}$ at $C_{naph} = 5\times10^{-4}$ and $1 < V_{EC} < 1.8\ \mu\mathrm{m\,s^{-1}}$ at $C_{naph} = 10^{-3}$, where the lower bounds are the highest value of V at which no EC's were observed and the higher bounds are the lowest value of V at which EC's appeared. The calculated values of V_{cs} for these concentrations are 1 and 0.6 $\mu\mathrm{m\,s^{-1}}$, respectively. The order of magnitude of V_{cs} is the same as that of V_{EC}, and both quantities vary with C_{naph} in the same way, as they should. The fact that the values of V_{cs} fall outside the experimental margin for V_{EC} is not significant since rough approximations were made in the calculation of V_{cs}.

EC patterns formed at $V \geqslant V_{EC}$ were observed to disappear when V was decreased below V_{EC}. No metastability range was positively observed. The range of metastability

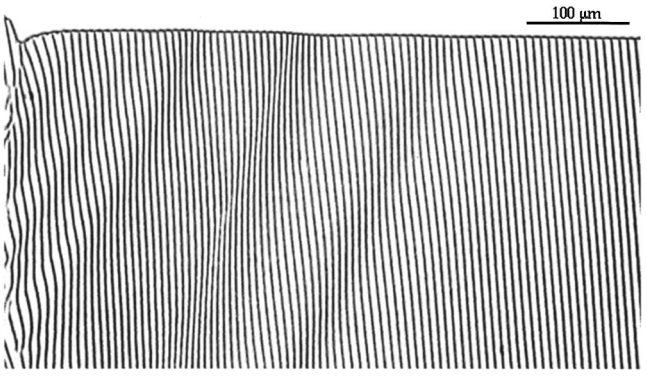

FIG. 10. Traveling waves. A grain boundary is located on the leftmost side of the figure ($C_{naph} = 2.5\times10^{-4}$; $V = 13.5\ \mu\mathrm{m\,s^{-1}}$).

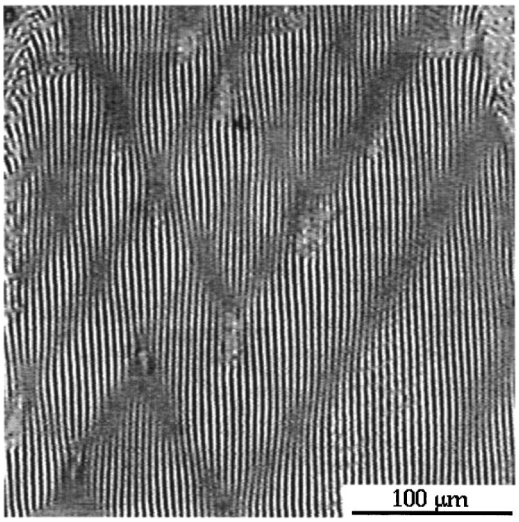

FIG. 11. Dense population of traveling waves at high velocity ($V=31\ \mu\mathrm{m\,s^{-1}}$). Undoped sample. The loss of contrast in the gray regions is due to three-dimensional instabilities.

between planar fronts and EC patterns is thus narrow (at most a few $\mu\mathrm{m\,s^{-1}}$ wide) at high impurity concentration, if it exists at all.

2. Process of formation of eutectic colonies

As already stated, V_{EC} was probably noticeably higher than the instability threshold velocity of the planar front in all the observed cases. In order to gain insight into the critical instabilities of the planar front, experimental runs consisting of subcritical V jumps (jumps from V_1 to V_2 with $V_1 < V_2 < V_{\mathrm{EC}}$), provoking a slight transitory overstepping of the threshold were carried out. The result of such a V jump performed in an undoped sample containing a relatively large concentration of residual gas is shown in Fig. 12. Similar observations were obtained in samples doped with naphthalene. Figure 12 clearly shows that the destabilization of the planar front rapidly gives rise to two-phase fingers consisting of a protruding β lamella sandwiched between to strongly deformed α lamellae (''α-β-α fingers''). Concerning the linear stage of the destabilization process, its short duration time, and the complications due to the nonuniform initial λ distribution prevented us from identifying the critical mode with certainty. It can only be stated that it is probably a nonoscillatory short-wavelength mode. Such modes as well as the two-phase fingers are incompatible with Cahn's rule.

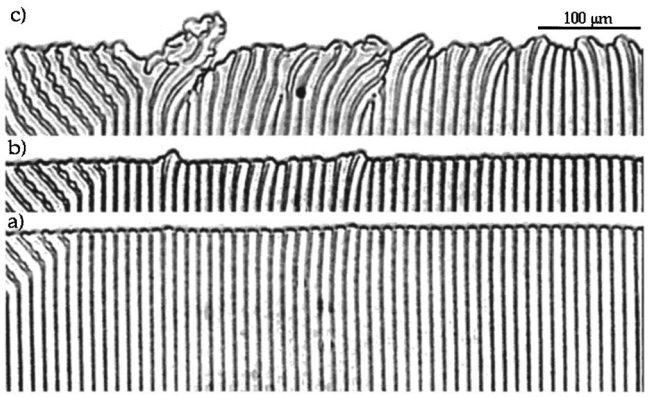

FIG. 12. Transient subsequent to a V jump from 3.1 to 5 $\mu\mathrm{m\,s^{-1}}$ in an undoped sample ($v=0.09$). (a) $t=41$ s, (b) 49 s, and (c) 59 s.

The typical course of the initial transients at $C_{\mathrm{naph}}=5\times10^{-4}$ and $V\geqslant V_{\mathrm{EC}}$ is illustrated in Fig. 6. Three distinct stages can be noted, corresponding to the successive appearance of TW's, two-phase fingers, and EC's, respectively. Each stage corresponds to a relatively large, sudden increase of the average temperature of the front, suggesting that the wavy front, the two-phase fingers, and the EC pattern are all stationary or quasistationary states of the system. The TW's appear a short time after the onset of the run, when the impurity concentration ahead of the front is still low, and do not substantially grow in amplitude, nor change their drift velocity afterwards, in agreement with the observations performed in low impurity concentration samples. The creation of two-phase fingers occurs when the transient is nearly completed, and follows a scenario which is not unique, but depends on the local λ distribution. The formation of EC's begins with the occurrence of lamella branching on the sides of the two-phase fingers. The transient is completed when the EC tips have reached their steady-state undercooling and the EC sides have come into contact with their neighbors.

Two different scenarios of creation of two-phase fingers appear in Fig. 6. In the largest part of the front, the two-phase fingers arise from the same destabilization process as in Fig. 12. In a small region of the front, in which the local value of λ was particularly large, the $2\lambda O$ mode of the lamellar pattern is excited, causing two-phase fingers and EC's to appear at a much shorter time than in the remainder of the front. The $2\lambda O$ mode is thus an efficient, but not a necessary, precursor of the formation of EC's. More importantly, the $2\lambda O$ mode leads to EC's only via the creation of two-phase fingers.

3. Two-phase fingers at off-eutectic concentrations

Figure 7 shows quasistable α-β-α fingers coexisting with EC's in a slightly hypoeutectic sample. The tip undercooling of the fingers is smaller than that of the EC's, contrary to what occurs at $v=0$. Such well-developed α-β-α fingers bear striking morphological and dynamical similarities with the symmetry-broken double fingers (''doublons'') of the low-anisotropy dilute-alloy solidification fronts [31,32]. Like the latter, they are constituted by two symmetrically disposed broad fingers of one phase separated by a thin lamella of another phase, and can change their growth direction without being destroyed (except by collision with another object). At still larger deviations from C_E, α-β-α fingers have been observed to compete with single-phase α dendrites.

A type of two-phase finger qualitatively different from the above α-β-α fingers is predominantly observed in slightly hypereutectic samples (Fig. 13). The sides of these fingers are occupied by the β phase, and the tips by several α lamellae separated from each other by β lamellae. The dynamical properties of these ''β-α-β multiplets'' are similar to those of the α-β-α fingers. Like the latter, they are reminiscent of structures observed in thin-sample directional solidification of dilute alloys [31–35].

4. Long-time dynamics of the eutectic-colony patterns

The dynamics of the permanent EC patterns as a function of V and v has not yet been studied in detail. However, all

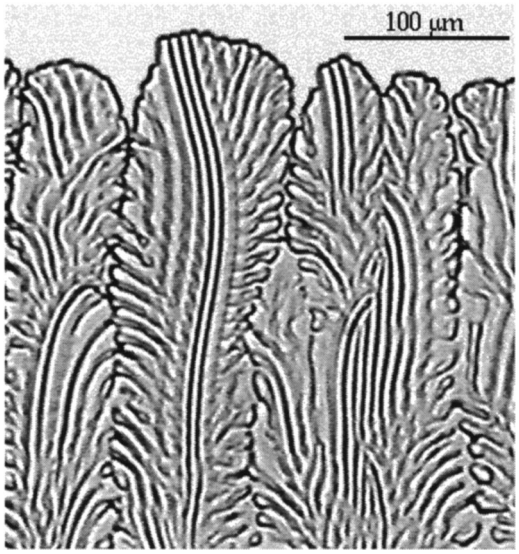

FIG. 13. Eutectic colonies and β-α-β multiplets. ($C_{\mathrm{naph}}=5\times10^{-4}$; $V=9.9\,\mu\mathrm{m\,s^{-1}}$).

the observations converge to show that EC patterns are unsteady. This is obviously the case at off-eutectic concentrations, as illustrated in Figs. 7 and 13, and also near the eutectic concentration. Figure 14 displays the spatiotemporal diagram of a near-eutectic EC pattern over a period of time much longer than τ_{naph}. For clarity, only the trajectories of the inter-EC grooves are represented. It can be seen that tip-splitting and squeezing-off events are taking place at a constant average frequency. However, it should be noted that most of these events concern short-lived grooves. The long-lived grooves are in small number ($\approx$9), and undergo only rare annihilation or creation events. The observations show that the short-lived grooves are shallow, while the long-lived ones are deep. This distinction between two types of grooves is further illustrated in Fig. 15, which shows the average EC spacing measured at different values of V in a given sample. Two largely different average values of the EC spacing are obtained depending on whether the shallow grooves are taken into account, or not.

Unsteady ''seaweed'' and shallow-cell patterns are observed in thin-sample directional solidification of dilute alloys when the anisotropy of the interfacial properties is low [31–36]. Thus the unsteadiness of the EC patterns is not an exceptional phenomenon. At off-eutectic concentrations, it certainly has to do with the peculiar dynamical properties of the two-phase fingers and multiplets, but this is less clear at near-eutectic concentrations.

5. Comparison with theory

Broadly speaking, the above observations are compatible with Plapp and Karma's theoretical results. We observe that the planar front is unstable above a velocity of the same order of magnitude as V_{cs}, and that both long-wavelength drifting modes and short-wavelength modes are involved in the destabilization process. The latter actually play a largely predominant part, a possibility which was not rejected by Plapp and Karma. The only apparent discrepancy concerns the nature of the critical mode. We find that this mode is not the $2\lambda O$ mode, but a nonoscillatory mode which had not been noted previously, to our best knowledge. That such a discrepancy arises is not a complete surprise, however, since all the modes incompatible with Cahn's rule are eliminated from Plapp and Karma's calculation.

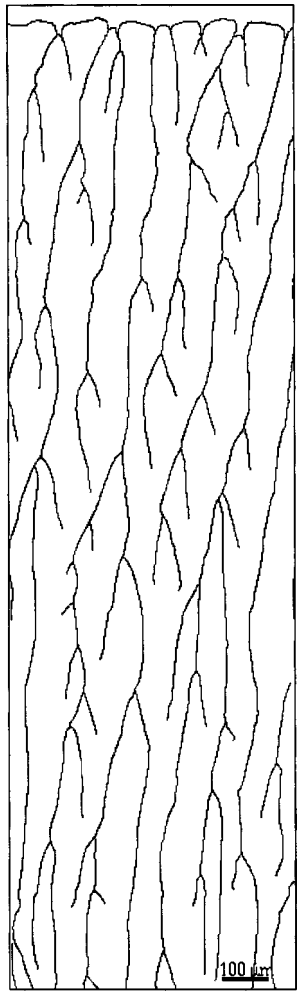

FIG. 14. Spatiotemporal diagram of an EC pattern (same run as in Fig. 2). Only the trajectories of the inter-EC liquid grooves are shown.

On the other hand, the transition from planar front to EC's is clearly not a continuous one. It is mediated by at least two

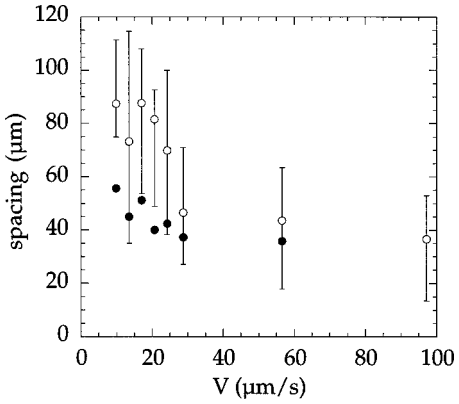

FIG. 15. Average EC spacing as a function of V measured taking account of deep liquid grooves only (open symbols; error bars: minimum and maximum measured values), or both deep and shallow grooves (filled symbols). $C_{\mathrm{naph}}=5\times10^{-4}$.

phenomena, namely, the formation of two-phase fingers, and the occurrence of lamella branching. The intermediate transition from planar front to two-phase fingers is perhaps continuous, i.e., it may correspond to a bifurcation of the system. In this case, the onset of the above-mentioned nonoscillatory mode would correspond to the (upper) bifurcation threshold. The existence of an alternative way of reaching the two-phase finger branch via the $2\lambda O$ mode pleads for a subcritical character of this bifurcation. This is not proven, however. It should also be noted that lamella branching results from 3D processes which are not yet fully understood, but are certain to depend on the sample thickness, and the wetting conditions at the glass plates [9,10]. It is therefore conceivable that lamella branching would occur earlier in samples thicker than ours, or in another alloy than CBr_4-C_2Cl_6, and would hide the other stages of the process.

C. Low impurity concentration

1. Transition to wavy fronts

At $C_{\mathrm{naph}}=2.5\times10^{-4}$ as well as in samples without naphthalene (but with residual impurities), TW's are observed to appear near eutectic grain boundaries above a certain velocity V_{TW}. The emitted TW's are not isolated, but are part of more or less continuous wave trains (Fig. 10). Given that long-wavelength perturbations are continually generated in the vicinity of eutectic grain boundaries (see Sec. II B 3), the obvious meaning of this observation is that long-wavelength perturbations spontaneously drift when $V\geqslant V_{\mathrm{TW}}$. Some eutectic grain boundaries are much more efficient than others as sources of TW's. This is connected with the frequency of the lamella termination, or branching events occurring at the boundary, which depends on the misorientation of the adjacent grains. Incidentally, the outer boundaries of the sample, i.e., the lines of contact of the alloy with the plastic spacers, also are active sources of TW's.

Within experimental uncertainty, the transition is abrupt (no TW's are observed below V_{TW}). The value of the drift angle $\psi=\tan^{-1}W/V$, where W is the drift velocity, is finite at V_{TW} and remains essentially constant as V increases. However, it must be kept in mind that V_{TW} is certainly larger than the actual transition velocity, so that the dependence of ψ on V in the vicinity of the transition is unknown. The observed values of ψ range from about 25° to 30°.

Substantially different values of the transition velocity were found in different samples with the same nominal concentration of naphthalene. This large dispersion is not entirely attributable to the small number of values of V explored in each sample. It is mostly due to the fact that V_{TW} increases very rapidly as the impurity concentration goes to zero, and is therefore very sensitive to the unwanted variations of C_X from a sample to another. In some well outgased undoped samples, no TW's were observed at any V, except during post-jump transients, showing that V_{TW} was higher than 31 $\mu\mathrm{m\,s^{-1}}$. On the other hand, the lowest value of V_{TW} found in the samples with $C_{\mathrm{naph}}=2.5\times10^{-4}$ was of 5 $\mu\mathrm{m\,s^{-1}}$. This value is comparable to the calculated value of V_{cs} for this concentration of naphthalene, and $C_X=4\times10^{-4}$.

The planar fronts remain robust against the formation of structures of larger amplitude than the TW's up to the maximum explored velocity, i.e., at least $6V_{\mathrm{cs}}$. This was tested by applying upward V jumps to wavy fronts. Low amplitude V jumps had no effect. Stronger V jumps resulted in the appearance of shallow EC patterns, i.e., patterns in which the depth of the inter-EC grooves was only of a few λ (Fig. 9). These shallow EC patterns spontaneously disappeared below a value of V comparable with V_{TW}. The whole range in V above V_{TW} can thus be considered as a metastability range between planar, or wavy fronts and shallow EC's.

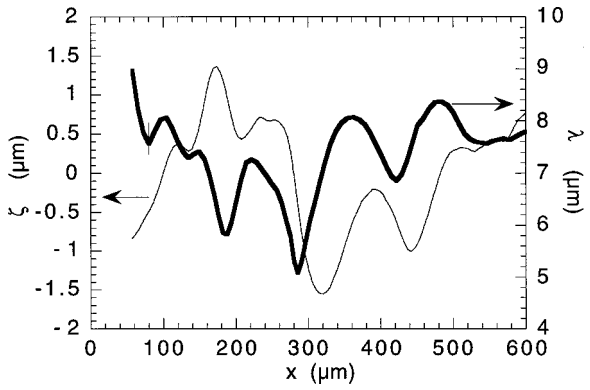

FIG. 16. Spacing distribution $\lambda(x)$ (thick line) and front profile $\zeta(x)$ (thin line) of the growth front of Fig. 10.

2. Wavy fronts and Cahn's rule

In the presence of TW's, the tilting of the lamellae and the distortion of the front are sufficiently large for the validity of Cahn's rule to be directly studied. We define the local lamella tilt angle ϕ as the angle between the trajectory of the lamellae and the normal to the envelope of the front. Cahn's rule states that $\phi\equiv0$. In fact, the lamella tilt angle is generally different from zero even when the spacing is uniform and the front perfectly planar because of capillary anisotropy (see Sec. II B 3). Furthermore, this ''homogeneous'' tilt angle generally is an increasing function of λ. It is thus natural to recast Cahn's rule as

$$\phi(x)=\phi_{\mathrm{hom}}[\lambda(x)], \tag{4}$$

where $\phi_{\mathrm{hom}}(\lambda)$ is the lamella tilt angle of a homogeneous pattern of spacing λ. This equation means that the lamellar pattern is locally the same as it would be if the spacing was uniform and the front was normal to the gradient. The two questions to be considered are: Is Eq. (4) verified in the experiment? Does the nonzero term on the right-hand side of Eq. (4) make a difference as concerns the dynamics of the TW's?

The $\lambda(x)$ and $\zeta(x)$ plots measured along the front of Fig. 10 are displayed in Fig. 16. The azimuthal angles (angles with respect to z) of the trajectories of the lamellae (θ) and the normal to the envelope of the front (τ) are plotted in Fig. 17. The plot of ϕ as a function of λ obtained by eliminating the variable x between $\lambda(x)$ and $\phi(x)=\theta(x)-\tau(x)$ is shown in Fig. 18. A second-order polynomial fitted to the data of Fig. 18 is similar to the previously found $\phi_{\mathrm{hom}}(\lambda)$ curves [9,37]. Similar results were obtained with other samples, allowing us to conclude that wavy fronts obey the generalized form of Cahn's rule represented by Eq. (4) within experimental uncertainty. Other observations (not re-

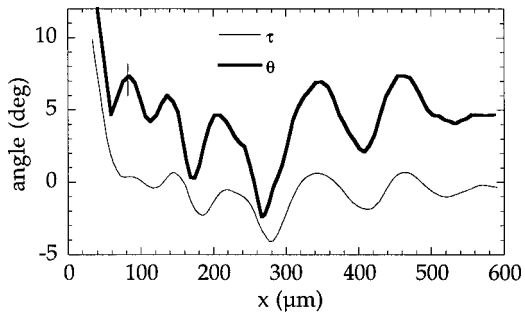

FIG. 17. Azimuthal angle of the lamellae (θ) and of the normal to the envelope (τ) of the growth front of Fig. 10.

produced) have shown that noticeable deviations from this equation are observed in the presence of large λ gradients.

Within a given grain, no marked difference is observed between the properties (drift velocity, λ profile) of rightward and leftward TW's. The specific effect of capillary anisotropy is to break the right-left symmetry, as shows up in the tilt of the lamellae. Since no such symmetry breaking is observed in the properties of the TW's, we conclude that the influence of a small capillary anisotropy—thus of the term $\phi_{\mathrm{hom}}(\lambda)$ in Eq. (4)—on the dynamics of the wavy fronts is negligible.

3. Isolated traveling waves

Figure 19 shows a time series of λ plots measured through the wave train of Fig. 10. The λ plots are represented in the reference frame attached to the wave ($\psi \approx 24°$). The amplitudes of the secondary maxima decrease much more rapidly than that of the principal maximum, so that only an isolated TW finally survives. This isolated wave has an asymmetric profile with a width of about 16 $\langle\lambda\rangle$. Such a profile is a reproducible feature of the isolated TW's, as will be shown shortly. Near the end of the recording, the standard deviation of the λ distribution decreases with a damping rate of about 0.02 s^{-1}. This rate is low compared to the phase diffusion damping rate calculated for the characteristic wavelength of 16 $\langle\lambda\rangle$ ($\approx 0.4\ s^{-1}$).

Figure 20 shows an isolated TW emitted a mechanism to be described below [see Fig. 23(b)], and Fig. 21 the corresponding λ plots. The λ profile of this wave is quite similar to the one appearing in Fig. 19. The standard deviation of the λ distribution first decreases with a damping rate of about 0.05 s^{-1}, and then reaches a plateau. The corresponding

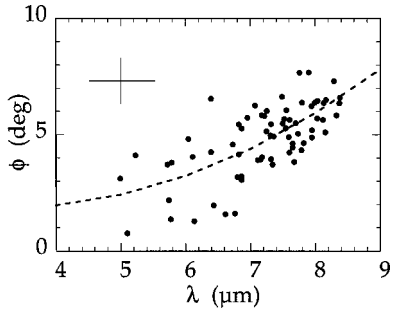

FIG. 18. Lamella tilt angle $\phi = \theta - \tau$ vs spacing λ. Symbols: experimental values from Figs. 16 and 17. Broken line: second order polynomial fit. $\lambda_{\mathrm{JH}} = 4.0\ \mu$m.

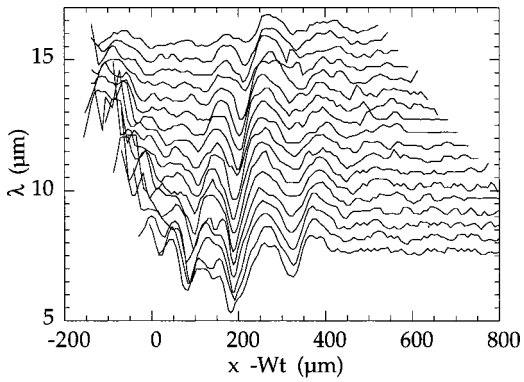

FIG. 19. λ plots measured at time intervals of 3.95 s represented in the reference frame drifting at the velocity $W = 6\ \mu\mathrm{m\,s^{-1}}$. Same run as in Fig. 10. Each plot has been shifted upwards with respect to the preceding one by 0.5 μm.

phase diffusion damping rate would be of about 3 s^{-1}. The plateau signals the existence of a permanent background of low amplitude waves, the detailed structure of which is not resolved.

The reproducible features of the isolated TW's (drift velocity, λ profile, and slow damping rate) raise the question of the possible existence of solitary waves. The observed TW's are clearly not solitary waves, but are perhaps close to a solitary wave at the moment of their creation. In any case, they are certain to be strongly nonlinear objects, as shown by the complex evolution of the λ profiles of the wave trains.

4. Dense populations of traveling waves

The TW's are a boundary condition dependent phenomenon. This is clearly illustrated in Fig. 8, which shows the central part of a large grain free of TW's at a high V in a sample doped with naphthalene. In smaller grains, however, the front is generally continually swept by rightward and

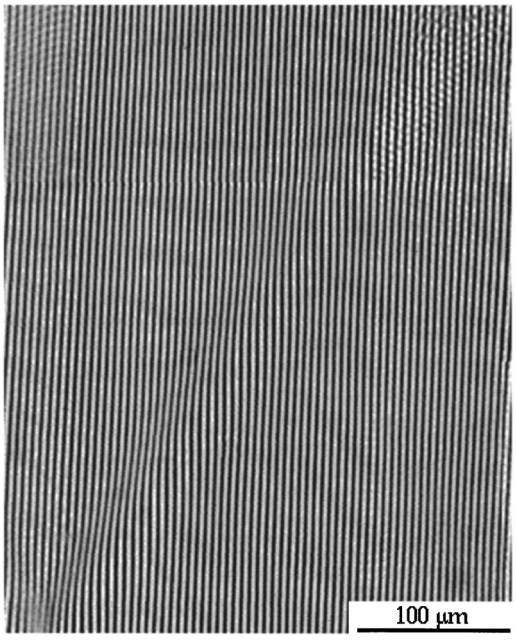

FIG. 20. Isolated traveling wave. $V = 31\ \mu\mathrm{m\,s^{-1}}$. $C_{\mathrm{naph}} = 2.5 \times 10^{-4}$.

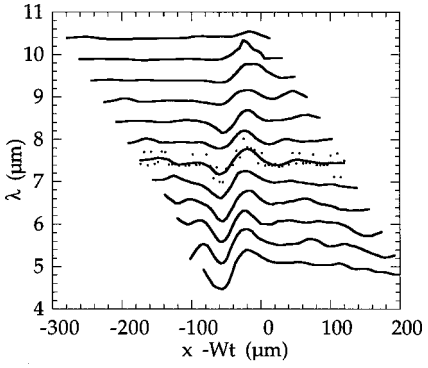

FIG. 21. λ plots measured at time intervals of 1.05 s represented in the reference frame drifting at $W=19.5\ \mu\mathrm{m\,s}^{-1}$. Same run as in Fig. 20. The data points of one of the plots are shown to illustrate the smoothing procedure. Each plot has been shifted upwards with respect to the preceding one by 1 μm.

leftward wave trains originating from the two boundaries. The resulting pattern resembles (but is not really) standing waves (Fig. 11). In fact, the interactions between TW's are highly nonlinear. This is illustrated in Fig. 22, which shows two different interaction processes between TW's observed during the same experimental run. The corresponding time series of λ plots are displayed in Fig. 23. In one case [Fig. 23(a)], two TW's of slightly different amplitudes meet. The amplitudes and the trajectories of the TW's are changed during the crossing process, the weakest of the two being further damped down. In the other case [Fig. 23(b)], a low-amplitude leftward TW is strongly amplified through the crossing with a large-amplitude rightward TW. The amplification mechanism involves an oscillatory mode of instability of the lamellar pattern and a lamella branching event. Similar short-frequency oscillations are observed in Fig. 23(a). This type of oscillation was not observed previously, and is probably a 3D mode of instability occurring when λ is much smaller than the sample thickness, thus at high V.

5. Shallow eutectic colonies

A typical feature of the shallow EC patterns is the existence of extremely wide long-lived EC's (Fig. 9). These large EC's do not seem subjected to tip splitting in the usual sense of the term (the front profile shows no detectable trough near the center of the EC's). This suggests that one should consider the shallow inter-EC grooves as localized entities, and the tip of the wide EC's as portions of an extended metastable wavy front. Thus considered, each groove

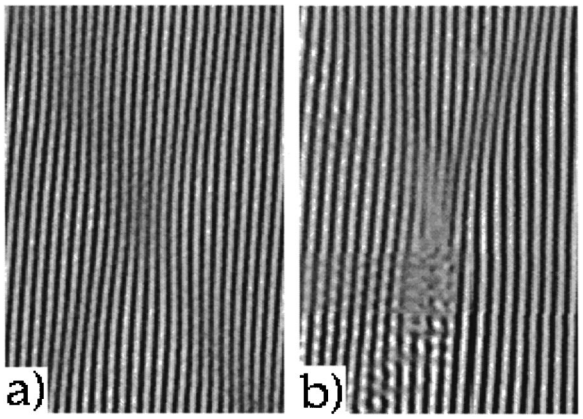

FIG. 22. Two different examples of TW crossings (same run as in Fig. 20). Each image is 113 μm wide.

is a defect containing a lamella sink and two lamella sources operating at the same average frequency (so that the average number of lamellae remains constant), and bound together by the Cahn distortion of the front. Symmetrical, stationary inter-EC grooves as well as asymmetrical, traveling ones are observed. The traveling velocity of the latter does not seem to be unique, which obviously implies that the pattern as a whole is unsteady.

Shallow inter-EC grooves are active sources of TW's (Fig. 9). The tips of the shallow EC's are therefore permanently occupied by a particularly dense population of TW's. This sometimes results in the creation of a new groove at the tip of an EC. The detailed mechanism of these rare, nonstandard tip-splitting events has not been elucidated. It can only be stated that lamella termination and lamella branching events are not rare in wavy fronts, but are most generally healed up by the emission or absorption of a TW [See Fig. 23(b)], and are therefore not the only cause of the occurrence of tip splitting events.

The same nonelucidated mechanism may give rise to a process of nucleation and invasion of wavy fronts by shallow EC's starting from eutectic grain boundaries. In this process, a first inter-EC groove is created at some distance of a eutectic grain boundary by the emitted TW's, a second inter-EC groove is created by the TW's emitted by the first inter-EC groove, and so on. This process was actually observed in a few experimental runs, and was extremely slow.

6. Comparison with theory

The observed TW's share many important features with the critical long-wavelength modes found by Plapp and

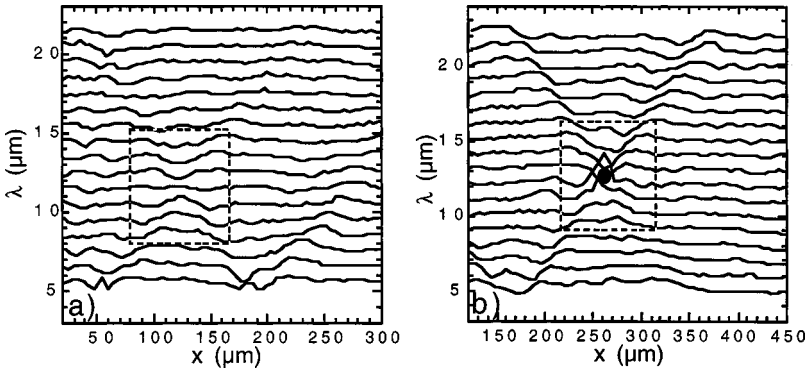

FIG. 23. Time series of λ plots for Fig. 22(a) (a) and Fig. 22(b) (b). Time interval: 0.54 s. Upward shift: 1 μm. Dotted lines: frames of Figs. 22(a) and 22(b). Filled circle: lamella branching.

Karma: the TW's obey Cahn's rule, appear at values of V comparable to V_{cs}, and have the same order of magnitude of their characteristic width and drift velocity as the calculated long-wavelength modes. Moreover, as already stated, $\Omega(k)$, as calculated by Plapp and Karma, is probably complex in the conditions in which the TW's are observed. Thus the basic mechanism responsible for the drift of the TW's most probably is the one pointed out by these authors, namely, the interaction between the distortions of the envelope and those of the lamellar pattern embodied in Cahn's rule. The fact that the TWs are only emitted by strong external perturbations, and fade out progressively afterward, shows that the experimentally measured transition velocity V_{TW} is not the critical velocity for the Plapp-Karma long-wavelength mode, but a lower velocity, below which the imaginary part of Ω is zero, and above which it is nonzero.

On the other hand, several aspects of the observations remain unexplained, in particular, the fact that the TW's do not amplify even at velocities much higher than V_{TW}. As far as we can see, the only theoretical clue to this spectacular stabilization of the planar front is the rapid rise of the effective capillary correction term as the impurity concentration decreases from 5 to 2.5×10^{-4} (see Sec. II B).

VI. CONCLUSION

This study has brought to light the specific features of the transition to eutectic colonies in ternary lamellar eutectics compared to the transition to cells in dilute alloys. These features stem from the interaction between the dynamics of the lamellar pattern and the large-scale impurity-driven cellulation process of the front. As far as long-wavelength distortions of the front are concerned, this interaction is well described by Cahn's rule, which must, however, be amended in order to take into account the tilt of the lamellae due to capillary anisotropy and spontaneous symmetry breaking. A consequence of Cahn's rule recently asserted by Plapp and Karma is that long-wavelength distortions of the front drift laterally above a certain velocity when the interlamellar spacing is sufficiently large. We have observed traveling waves, which, although highly nonlinear, are most probably due to this effect.

However, the main contribution of this study probably consists of a series of unexpected facts, the most important of which are the following: the transition to EC's is not continuous, but mediated by a first transition to a new type of dynamical structure called two-phase finger, similar to the doublon and multiplet observed in directionally solidified low-anisotropy dilute alloys; the transition to EC's disappears relatively abruptly as the impurity concentration decreases; at low impurity concentration, strongly metastable wavy fronts (i.e., planar front swept by traveling waves) are observed over a large range in velocity above a certain threshold value. Further studies are in progress concerning, in particular, the properties of the two-phase fingers at slightly off-eutectic concentrations.

ACKNOWLEDGMENTS

We gratefully acknowledge many stimulating discussions with A. Karma and M. Plapp, and thank them for communicating their results prior to publication. Thanks are also due to H. Savary and A.-M. Pougnet, of the Centre National d'Etudes des Télécommunications, France-Telecom, Bagneux, France, for providing us with zone-refined chemicals. This research was financially supported by the Center National d'Etudes Spatiales, France.

[1] W. Kurz and D. J. Fischer, in *Fundamentals of solidification* (Trans. Tech, Aedermannsdorf, 1984), p. 93.
[2] J. D. Hunt and K. A. Jackson, Trans. AIME **236**, 843 (1966).
[3] K. A. Jackson and J. D. Hunt, Trans. AIME **236**, 1129 (1966).
[4] W. Datye and J. S. Langer, Phys. Rev. B **24**, 4155 (1981); see also J. S. Langer, Phys. Rev. Lett. **44**, 1023 (1980).
[5] A. Karma, Phys. Rev. Lett. **59**, 71 (1987).
[6] A. Karma and A. Sarkissian, Metall. Mater. Trans. A **27**, 635 (1996).
[7] K. Kassner and C. Misbah, Phys. Rev. A **44**, 6533 (1991).
[8] K. Kassner, C. Misbah, and R. Bauman, Phys. Rev. E **51**, R2751 (1995).
[9] G. Faivre and J. Mergy, Phys. Rev. A **45**, 7320 (1992); **46**, 963 (1992); also see J. Mergy, Thèse de l' Université Paris VII, France, 1992 (unpublished).
[10] M. Ginibre, S. Akamatsu, and G. Faivre, Phys. Rev. E **56**, 780 (1997); also see M. Ginibre, Thèse de l' Université Paris VI, France, 1997 (unpublished).
[11] For simplicity, we ignore here the distinction between impurities (unwanted or uncontrolled chemical components) and addition components (intentionally added species).
[12] W. H. Weart and J. D. Mack, Trans. Metall. Soc. AIME **236**, 1129 (1958).
[13] J. P. Chilton and W. C. Winegard, J. Inst. Met. **89**, 16 (1961).
[14] J. E. Gruzleski and W. C. Winegard, J. Inst. Met. **96**, 304 (1968); Trans. AIME **242**, 1785 (1968).
[15] M. D. Rinaldi, R. M. Sharp, and M. C. Flemings, Metall. Trans. **3**, 3133 (1972).
[16] J. W. Rutter and B. Chalmers, Can. J. Phys. **31**, 15 (1953); see also W. A. Tiller, K. A. Jackson, J. W. Rutter, and B. Chalmers, Acta Metall. **1**, 498 (1953).
[17] W. W. Mullins and R. F. Sekerka, J. Appl. Phys. **35**, 444 (1964).
[18] In a binary dilute alloy, V_{cs} is defined as the value of V above which the liquid ahead of the front is supersaturated with respect to the solute [16]. This definition can be extended to multicomponent eutectic alloys by averaging the concentrations along the direction perpendicular to the lamellae [15].
[19] The experimental fact that, in the EC patterns, the trajectories of the lamellae run (approximately) perpendicular to the envelope of the deformed front was apparently first noted by Weart and Mack [12]. On the other hand, according to Jackson and Hunt [3], Cahn was the first to make the assumption that this rule was verified in all cases (i.e., also in the absence of EC's), and point out the consequences of this hypothesis. Here we primarily use the term of Cahn's rule in reference to experimental observations.
[20] W. Losert, B. Q. Shi, and H. Z. Cummins, Proc. Natl. Acad.

Sci. USA **95**, 431 (1998); **95**, 439 (1998).
[21] M. Plapp and A. Karma, Phys. Rev. E **60**, 6865 (1999).
[22] W. L. Kaukler and J. W. Rutter, Mater. Sci. Eng. **65**, L1 (1984).
[23] V. Seetharaman and R. Trivedi, Metall. Trans. A **19**, 2955 (1988).
[24] R. Trivedi, J. T. Mason, J. D. Verhoeven, and W. Kurz, Metall. Trans. A **22**, 2523 (1991).
[25] B. Caroli, C. Caroli, G. Faivre, and J. Mergy, J. Cryst. Growth **118**, 135 (1992).
[26] J. Mergy, G. Faivre, C. Guthmann, and R. Mellet, J. Cryst. Growth **134**, 353 (1993).
[27] L. M. Hogan, R. W. Kraft, and F. D. Lemkey, Adv. Mater. Res. (N.Y.) **5**, 83 (1971).
[28] We use the public domain NIH Image program (developed at the U.S. National Institutes of Health and available from Internet by anonymous FTP from zippy.nimh.nih.gov or on floppy disk from the National Technical Information Service, Springfield, Virginia, part No. PB95-500195GEI).
[29] S. Akamatsu and G. Faivre, J. Phys. I **6**, 503 (1996).
[30] V. G. Smith, W. A. Tiller, and J. W. Rutter, Can. J. Phys. **33**, 723 (1955); also see B. Caroli, C. Caroli, and L. Ramirez-Piscina, J. Cryst. Growth **132**, 377 (1993).
[31] T. Ihle and H. Müller-Krumbhaar, Phys. Rev. E **49**, 2972 (1994).
[32] S. Akamatsu, G. Faivre, and T. Ihle, Phys. Rev. E **51**, 4751 (1995).
[33] H. Jamgotchian, R. Trivedi, and B. Billia, Phys. Rev. E **47**, 4313 (1993).
[34] W. Losert, D. A. Stillman, H. Z. Cummins, P. Kopczynski, W.-J. Rappel, and A. Karma, Phys. Rev. E **58**, 7492 (1998).
[35] P. Kopczynski, W. J. Rappel, and A. Karma, Phys. Rev. Lett. **77**, 3387 (1996); **79**, 2698 (1997).
[36] S. Akamatsu and G. Faivre, Phys. Rev. E **58**, 3302 (1998).
[37] K. Kassner and C. Misbah, Phys. Rev. A **45**, 7372 (1992).